Radiation, temperatuur, and leaf area explain ecosystem carbon fluxes in boreal and temperate European forests

van Dijk, A.I.J.M.; Dolman, A.J.; Schulze, E.D.

published in
Global Biogeochemical Cycles
2005

DOI (link to publisher)
10.1029/2004GB002417

document version
Publisher's PDF, also known as Version of record

Radiation, temperature, and leaf area explain ecosystem carbon fluxes in boreal and temperate European forests

Albert I. J. M. van Dijk[1] and A. J. Dolman

Department of Hydrology and Geo-Environmental Sciences, Faculty of Earth and Life Sciences, Vrije Universiteit Amsterdam, Amsterdam, Netherlands

Ernst-Detlef Schulze

Max Planck Institute for Biogeochemistry, Jena, Germany

Received 23 November 2004; revised 22 February 2005; accepted 7 April 2005; published 22 June 2005.

[1] We analyzed measurements of net ecosystem exchange of CO_2 (NEE) over 15 European forests (the EuroFlux data set) to investigate which climate and forest characteristics explain temporal and intersite variations in NEE and its components, gross primary production (GPP) and respiration (R). Informed stepwise regression was used to derive a parameter-efficient, empirical model that was consistent with process knowledge. The resulting model required seven site-specific parameters to describe flux behavior at different temporal scales as a function of radiation, temperature, and air humidity. The interpretation appeared robust despite method and data uncertainties, although the data set was probably biased toward well-watered boreal and temperate European forests. Radiation, temperature, and leaf area (through forest assimilation capacity) appear to be the main drivers of the observed temporal and intersite variation in gross primary production, ecosystem respiration, and net ecosystem exchange.

Citation: van Dijk, A. I. J. M., A. J. Dolman, and E.-D. Schulze (2005), Radiation, temperature, and leaf area explain ecosystem carbon fluxes in boreal and temperate European forests, *Global Biogeochem. Cycles*, *19*, GB2029, doi:10.1029/2004GB002417.

1. Introduction

[2] European forests are sequestering carbon and therefore play an important role in the continental and global carbon cycle [e.g., *Intergovernmental Panel on Climate Change* (*IPCC*), 2001; *Janssens et al.*, 2003]. Unfortunately, the exact magnitude of carbon uptake and the factors that control this apparent sink are still largely unclear. A better understanding of the main factors causing differences in net ecosystem exchange of CO_2 (NEE) among European forests, but also its variation in time, is needed to arrive at more reliable regional and national carbon budgets, and to understand how the forest carbon sink might behave in future.

[3] Eddy covariance measurements of NEE have been made by members of the EuroFlux project since 1996 over 15 mainly mature and extensively managed European forests. The original measurements suggest a latitudinal trend in annual NEE, with an approximately neutral budget or small net release for northern boreal forests, to significant uptake for forests southwards [*Valentini et al.*, 2000]. NEE is the balance between two large terms: ecosystem respiration (R) and gross primary production (GPP). Until recently, it was unclear how both terms change with latitude, that is, whether the southward NEE increase is caused by an R decrease [*Valentini et al.*, 2000], a GPP increase [*Janssens et al.*, 2001], or both. Recent estimates of GPP and R based on the EuroFlux data suggest that GPP increases southward more rapidly than R [*Van Dijk and Dolman*, 2004].

[4] Latitude can only be expected to be a surrogate for real drivers such as radiation, temperature, growing season, and water balance. Differences in NEE brought about by climate are confounded by site-specific properties of the forest stand and soil and their management [*Nabuurs et al.*, 2002]. Being able to separate climate and site-specific factors is important for understanding the effect of changes in climate, for evaluating the potential for increased uptake through forest management, and for establishing ''business-as-usual'' reference scenarios to evaluate such measures [*IPCC*, 2001].

[5] We analyzed the NEE data collected by EuroFlux members from 1996 to 2000, with specific attention to the following questions: (1) What is the relative importance of different climate and forest characteristics in determining GPP, R and NEE? (2) What fraction of the temporal variability in GPP, R and NEE, on timescales varying between half hours to multiple years, can be explained by variations in climate? From here on, we will use F_{NEE} in $\mu mol\ m^{-2}\ s^{-1}$ for instantaneous NEE fluxes (typically half-hourly means) and NEE for the concept itself, or for fluxes integrated over longer timescales (typically in t C $ha^{-1}\ yr^{-1}$); likewise for GPP and R. Furthermore, all fluxes and parameters are expressed per unit ground area, and

[1] Now at CSIRO Land and Water, Canberra, ACT, Australia.

0886-6236/05/2004GB002417$12.00

following micrometeorological convention, a negative flux indicates uptake from the atmosphere, and a positive flux release to it.

[6] Using the EuroFlux F_{NEE} data processed by *Falge et al.* [2001], we first estimated F_{GPP} and F_R by interpolating nighttime F_R measurements to daytime conditions using the well-established relationship between temperature and F_R. This was combined with an analysis of the spatial and temporal variation in the parameter that defines this relationship, Q_{10} (reported by *Van Dijk and Dolman* [2004]; summarized in section 2.2). The present paper describes a model-assisted analysis of the temporal and intersite variation of the resulting F_{GPP} and F_R estimates, and how these relate to climate and forest characteristics. There are alternative ways to do this analysis, each with strengths and weaknesses. A purely statistical, ''top-down'' approach can ensure a minimum of parameters and is robust, but may not allow process interpretation or can even be at odds with existing understanding. Conversely, ''bottom-up'' ecosystem process models incorporate physiological knowledge and (more or less) validated models, but these component models are not necessarily suitable for integration or the scale and type of measurements available. Despite their important other roles in carbon cycle research, such models typically also have too many parameters, and associated parameter identifiability problems, to allow meaningful data analysis and interpretation [cf. *Knorr and Heimann*, 2001; *Sitch et al.*, 2003]. With the intention of combining the strengths of the respective approaches, we followed the intermediate approach of performing an informed stepwise regression analysis, yielding a physiologically sound model, but with a minimal number of parameters needed to explain observed patterns, and so offering the best prospects for robust interpretation. We aimed to detect the main drivers of temporal and intersite variability in fluxes, rather than to develop and validate a new process model. Independent calibration and validation were therefore not attempted, and the results should be interpreted in the vein of previous data analyses [e.g., *Falge et al.*, 2002]. To identify the most important factors explaining NEE differences among sites, the parameter uncertainty, sensitivity, and intersite variability were investigated and where possible linked to site characteristics.

2. Materials and Methods

2.1. Data Selection

[7] The method by which the eddy covariance NEE measurements were carried out is described by *Aubinet et al.* [2000]. The ecosystems studied include 10 forests dominated by pine and spruce (*Pinus* spp., *Picea* spp.) at latitudes between Finland and southwestern France; beech (*Fagus sylvatica*) forests in Denmark, northern France, and upland Italy; a holm oak (*Quercus ilex*) forest in central Italy; and a cottonwood (*Populus trichocarpa*) forest in Iceland [*Valentini*, 2003]. The data set has been extended and reprocessed for some sites since the earliest reports [e.g., *Valentini et al.*, 2000]. This has led to some differences in reported fluxes. We used the half-hourly F_{NEE} data set compiled by *Falge et al.* [2001] that was available from the EuroFlux network, but only used original (i.e., not gap-filled) data. We further omitted data that might have been affected by low wind speeds, using site-specific friction velocity (u^*) thresholds determined by *Falge et al.* [2001] (0–0.47 m s^{-1}). There was a likely but unconfirmed unit conversion error in the data from Norunda (Sweden). We could still analyze these data, but did not include the results where this might affect our conclusions.

2.2. Daytime GPP and R Separation

[8] A separation between F_{GPP} and F_R can be made on the assumption that F_{GPP} does not occur during nighttime and that systematic diurnal variations in F_R are caused by temperature (measured at a chosen reference level above or below the soil surface, T in °C). Under these assumptions, F_R can be interpolated to daytime conditions and F_{GPP} is subsequently found as the difference between observed F_{NEE} and estimated F_R. An exponential equation describes the relationship between instantaneous $F_R(i)$ and $T(i)$,

$$F_R(i) = R_0(j)\exp[\beta T(i)], \quad (1)$$

where $R_0(j)$ (μmol m^{-2} s^{-1}, in this case estimated for day j) is the base respiration rate (i.e., respiration normalized to 0°C) and β (°C^{-1}) is an empirical exponent. Equation (1) is equivalent to a so-called Q_{10} function, where Q_{10} is the relative respiration increase after every 10°C temperature rise and equal to exp(10 β). Other, arguably more physically correct temperature response functions have been proposed [e.g., *Lloyd and Taylor*, 1994], but these normally have a very similar form over the observed temperature range, do not explain more of the observed variation, and because they have more fitting parameters, are more prone to parameterization problems.

[9] Total ecosystem respiration consists of heterotrophic respiration (mainly from litter and soil), and autotrophic respiration from living foliage, wood, and roots. All four sources are of comparable magnitude, but vary in importance between sites and seasons and can be expected to be driven by the temperature of the corresponding ecosystem compartments [*Högberg et al.*, 2001; *Bernhofer et al.*, 2003; *Falge et al.*, 2003; *Janssens et al.*, 2003; *Rebmann et al.*, 2004]. Because direct, unified, and continuous measurements of the respective fluxes and temperatures at ecosystem scale are not available for the EuroFlux data set, pragmatic choices have to be made in using equation (1). *Van Dijk and Dolman* [2004] showed that air temperature (measured above the canopy) yielded more consistent Q_{10} values than soil temperature, and also produced less uncertain GPP and R estimates [cf. *Carrara et al.*, 2004].

[10] Assumptions underlying equation (1) are that neither R_0 nor Q_{10} change over the period of interpolation, and therefore that sources of variation in respiration other than temperature (such as soil moisture, assimilation, and litter production) can be ignored. These assumptions are violated for a full year because of the seasonal course in R_0 and possibly also in Q_{10} [*Janssens and Pilegaard*, 2003] (but see *Van Dijk and Dolman* [2004]). The optimum timescale for using equation (1) represents a tradeoff between uncer-

Table 1. Summary of Location, Site Characteristics, and NEE Components for the 15 Sites[a]

		Site Characteristics						Exchange Components, t C ha^{-1} yr^{-1}			
Code	Site	Latitude, °N	T_{avg}, °C	Q_{avg}, GJ yr^{-1}	LAI	Number of Years	u^* Threshold, m s^{-1}	NEE	GPP	R	Species
FL	Flakaliden, Sweden	64.1	1.6	2.9	2	3	0	−1.1	−7.4	6.2	E (*Picea abies*)
GU	Gunnarsholt, Iceland	63.8	3.9	N/A	1.4	3	0.05	−1.8	−7.0	5.4	D (*Populus tr.*)
HY	Hyytiälä, Finland	61.9	3.4	2.8	3	5	0.26	−2.0	−11.0	9.0	E (*P. sylvestris*)
NO	Norunda, Sweden	60.1	4.0	3.5	5	3	0.31	(0.8)	(−7.6)	(8.4)	E (*P. sylvestris*)
AB	Aberfeldy, UK	56.6	7.3	3.2	8	2	0.31	−5.6	−19.6	14.0	E (*Picea abies*)
SO	Sorø, Denmark	55.5	7.2	3.4	4.8	4	0.23	−0.9	−16.8	15.9	D (*Fagus s.*)
LO	Loobos, Netherlands	52.2	9.0	3.4	3	4	0.20	−2.7	−16.2	13.5	E (*P. sylvestris*)
BR	Brasschaat Belgium	51.3	9.5	3.3	3	3	0.23	1.4	−12.9	14.4	E (*P. sylvestris*)
TH	Tharandt, Denmark	51.0	7.8	3.8	7.6	4	0.29	−6.5	−20.9	14.3	E (*Picea abies*)
VI	Vielsalm, Belgium	50.3	6.2	3.4	4.5	2	0.23	−4.7	−18.5	13.7	E/D (mixed)
WE	Weidenbrunnen, Denmark	50.2	5.7	3.5	5	4	0.41	0.3	−14.4	14.6	E (*Picea abies*)
HE	Hesse, France	48.7	8.8	3.9	6	5	0	−3.2	−17.5	14.3	D (*Fagus s.*)
BO	Bordeaux, France	44.1	11.8	5.0	5.5	3	0.22	−4.7	−19.1	14.4	E (*P. pinaster*)
CL	Collelongo, Italy	41.9	5.4	4.3	4	2	0.16	−7.3	−15.4	8.4	D (*Fagus s.*)
CP	Castelporziano, Italy	41.8	12.9	4.1	3.5	2	0.09	−5.2	−19.3	14.1	E (*Quercus ilex*)

[a]Listed are latitude, average annual temperature (T_{avg}) and radiation (Q_{avg}), leaf area index (LAI), the number of years of observation, and the determined threshold friction velocity threshold u^* [*Falge et al.*, 2001], as well as average annual net ecosystem exchange (NEE), gross primary production (GPP), and respiration (R) (estimated from NEE using $Q_{10} = 2.0$ and u^* friction thresholds found by *Falge et al.* [2001] and gap filled). Also listed are the dominant tree type (*E* for evergreen, *D* for deciduous) and species (*Populus tr.*, *Populus trichocarpa*; *P.*, *Pinus*; *Fagus s.*, *Fagus sylvatica*).

tainty in the estimate caused by sample size, and bias introduced by violation of this assumption. At a monthly timescale, *Van Dijk and Dolman* [2004] found Q_{10} values (for air temperature) varying between 1.6 and 2.5 for different sites, months, soil moisture conditions, statistical significance criteria, and friction velocity thresholds. However, the differences were not statistically significant or could be attributed to sample size or residual data bias [*Van Dijk and Dolman*, 2004]. While this is not to say that there is no Q_{10} variation in reality, these findings did not provide a statistical argument for using site- or season-specific values to estimate daytime F_{GPP} and F_R. Instead, the overall average Q_{10} value of 2.0 was used, and subsequently calculations were repeated with Q_{10} values of 1.5 and 3.5 to derive a conservative estimate of uncertainty. This led to annual R estimates that were an average 5% lower and 16% higher, respectively [*Van Dijk and Dolman*, 2004].

[11] First, we estimated $R_0(j)$ value for each night j (starting on day j) from n available half-hourly means of $F_{NEE}(i)$ and air temperature $T(i)$ as (see equation (1))

$$R_0(j) = \frac{1}{n}\sum \frac{F_{NEE}(i)}{\exp[\beta T(i)]}. \quad (2)$$

[12] We only calculated R_0 in this manner for nights with $n \geq 5$ (nighttime was defined as intervals without shortwave radiation, excluding the first half hour after sunset and last half hour before sunrise to exclude transition effects). Values of R_0 for remaining nights were estimated as the mean of $R_0(j-1)$ and $R_0(j+1)$. If either of these was not available, we took the mean for the two preceding and two following nights, and so on, up to 7 days before and after. Subsequently, we estimated F_R during daytime using equation (1) with air temperature measurements and the mean of $R_0(j-1)$ and $R_0(j)$.

[13] Ultimately, to obtain estimates of annual NEE, GPP, and R, missing values in the estimated F_{GPP} and F_R series were interpolated (gap-filled). The procedure followed was very similar to that used by *Falge et al.* [2001]. For gaps smaller than 3 hours in duration, half-hourly values were estimated as the mean of the mean fluxes over the three preceding and over the three following hours, respectively. For larger gaps, fluxes were estimated as the mean of the mean fluxes for this time of day on the three preceding and on the three following days, respectively. If this did not produce an estimate, we consecutively used the preceding and following 15, 30, and 60 days instead. If this still failed to produce an estimate, we used mean values for this day of the year and time of day for the full data set. However, when more than 50% of the data needed to be filled in by this latter method, we did not use the annual sums in subsequent calculations. The calculated mean annual NEE, GPP, and R for are listed together with climate and forest characteristics for each site in Table 1.

2.3. Model Description

[14] Original (not gap-filled) half-hourly F_{GPP} and F_R estimates were used in stepwise regression to construct a model including the main variables driving NEE. Where physiological knowledge was available, it was used to inform the order and type of model selection. Otherwise, the concept used was similar to Akaike's Information Criterion (AIC): A new model component was accepted if it explained at least 2% of additional variance in half-hourly GPP or R. Further details are given in Appendix A.

[15] The resulting model described F_{GPP} and F_R as a function of global radiation Q (W m^{-2}), above-canopy air temperature T (°C), mean air temperature during the preceding 21 days T_{21} (°C), and vapor pressure deficit D (kPa) for each half hour interval i (see *Aubinet et al.* [2000] for measurement details). The respective equations, in addition

to equation (1), are given below. F_{GPP} is modeled as [cf. *Hollinger et al.*, 1994]

$$F_{GPP}(i) = \frac{f_\alpha A_s(i) Q(i)}{[1 + f_\alpha Q(i)][1 + \gamma D(i)]}, \quad (3)$$

where f_α (0.0042 m^2 W^{-1}) is a ratio between ecosystem light use efficiency α (μmol J^{-1}) and light-saturated assimilation rate A_s (μmol m^{-2} s^{-1}) found by regression analysis (Appendix A), and γ (kPa^{-1}) is a fitting parameter defining the relationship between A_s and D [cf. *Schulze and Hall*, 1982; *Leuning*, 1995]. Stomatal control affects GPP by responding to air humidity; a response to soil water stress was not apparent from the data set, but may reflect a bias toward well-watered conditions [*Schulze*, 1986] (see Appendix A).

[16] The light-saturated assimilation rate (A_s) was best correlated to the mean temperature over the preceding period. An averaging period of 21 days gave the best overall results, although the optimum averaging period varied between sites (Appendix A). The seasonal change in assimilation capacity is described in a way that resembles the concept of cumulative degree days. In combination with the annual course in temperature, it produces the typical flattened bell shape that describes the phenology of both evergreen and deciduous forests [*Lechowicz*, 1984; *Goulden et al.*, 1996; *Barr et al.*, 2004],

$$A_s(i) = A_{s,\max}\left[\frac{1}{\pi}\arctan\Delta\left(T_{21}(i) - T_{21}^*\right) + \frac{1}{2}\right]. \quad (4)$$

The theoretical maximum assimilation rate $A_{s,\max}$ (μmol m^{-2} s^{-1}) is approached asymptotically at high T_{21} values; maximum transition rate Δ/π ($°C^{-1}$) is the maximum relative rate of change in A_s per degree change in T_{21}; and crossover temperature T_{21}^* is the temperature at which this maximum transition rate occurs (also $A_s/A_{s,\max} = 1/2$ at T_{21}^*). Equation (4) can be seen as a first, parameter-efficient approach to describe the response of phenology to temperature. In reality, other (often correlated) environmental conditions presumably also play a role.

[17] Base respiration R_0 was correlated to assimilation rate A_s but in many cases exhibited two domains: being apparently constant at low A_s and proportionally increasing beyond a threshold A_s (Appendix A) [cf. *Carrara et al.*, 2004]. This relationship was described by

$$R_0(i) = \max\left(R_{0,\min}, aA_s(i) + b\right), \quad (5)$$

where $R_{0,\min}$ ($\geq b$ μmol m^{-2} s^{-1}) is minimum base respiration, the coefficient a (≥ 0) is the slope of the function describing the rising part of the relationship, and b (μmol m^{-2} s^{-1}) is the y axis intercept. Base respiration R_0 starts to increase beyond a threshold value $A_s^* = (R_{0,\min} - b)/a$. Equation (5) can also describe situations in which R_0 simply increases monotonically with A_s (in which case $R_{0,\min} = b$ and A_s^* undefined) or is constant (if in addition $a = 0$).

[18] After F_{GPP} and F_R are calculated, net ecosystem exchange (F_{NEE}) follows from

$$F_{NEE}(i) = F_{GPP}(i) + F_R(i). \quad (6)$$

In total, therefore, the model uses three original input time series (Q, T, and D) and up to nine parameters (Q_{10}, f_α, $A_{s,\max}$, Δ, T_{21}^*, γ, $R_{0,\min}$, a, and b).

2.4. Data Analysis

[19] We nonlinearly optimized values for seven out of nine model parameters for each site to minimize the sum of squared differences between observed and modeled F_{NEE} values (F_{GPP} and F_R estimates were not used at this stage). An overall mean Q_{10} value of 2.0 was used (see section 2.2), and the assimilation parameter f_α was prescribed as a function of $A_{s,\max}$ (Appendix A) [cf. *Pilegaard et al.*, 2001; *Carrara et al.*, 2004]. Both parameters were included in subsequent uncertainty and sensitivity analysis, however.

[20] We evaluated the degree to which the seven fitted parameters together with climate explained flux behavior, by comparing the absolute and relative agreement between observed and modeled mean F_{NEE}, and by calculating Nash-Sutcliffe model efficiency (E),

$$E = \frac{\sigma_{obs}^2 - \sigma_{res}^2}{\sigma_{obs}^2}, \quad (7)$$

where σ_{obs}^2 represents the initial variance in observed F_{NEE} values and σ_{res}^2 is the residual variance (i.e., the sum of squared differences between observed and modeled values). The resulting E values describe how well plotted pairs of observed and modeled values cluster around the 1:1 line similar to the coefficient of determination (r^2). Negative values occur if model performance is poorer than if the mean F_{NEE} had simply been used.

[21] Time series of F_{NEE}, F_{GPP}, and F_R that were "observed" (the latter two were estimated from the first) and "modeled" (they were not modeled independently) were gap-filled using the method described before and integrated over daily, weekly, bi-weekly, monthly, and annual timescales. The resulting NEE, GPP, and R were compared, and E was also calculated at these timescales.

2.5. Parameter Testing

[22] For each parameter, the uncertainty, sensitivity and intersite variability were determined in order to investigate its importance in explaining NEE. Parameter uncertainty describes how well a parameter is defined. The effects of selected Q_{10} values and friction velocity (u^*) threshold on parameter uncertainty were conservatively estimated by refitting the model using Q_{10} values of 1.6 and 2.5 [cf. *Van Dijk and Dolman*, 2004], and u^* thresholds of 0 and 0.5 m s^{-1} [cf. *Falge et al.*, 2001]. The mean absolute change in each fitted parameter for all sites was divided by the mean of the original values (similar to a coefficient of variation), yielding an estimate of overall relative parameter uncertainty U. The mean change in the fraction of variance explained (in this case equal to the change in model efficiency E) was also determined, as well as the

Table 2. Fitted NEE Model Parameters and Indicators of Model Performance[a]

Site Code or Mean	Δ/π, °C $^{-1}$	T^*_{21}, °C	$A_{s,max}$, μmol m^{-2} s^{-1}	γ, kPa^{-1}	$R_{0,min}$, μmol m^{-2} s^{-1}	a	A^*_s, μmol m^{-2} s^{-1}	E	Modeled-Observed F_{NEE}, μmol m^{-2} s^{-1}	Modeled-Observed F_{NEE}, Percent of Mean
FL	0.45	0.3	15.1	0	1.04	0	n/d	0.62	−0.16	53
HY	0.07	7.6	31.1	0.005	0.71	0.059	7.9	0.83	−0.09	6
NO	0.08	4.8	(16.1)	0	(0.61)	0.075	(3.6)	0.74	(0.77)	29
WE	0.09	3.9	27.4	0	0.65	0.067	0	0.81	−0.22	24
VI	0.07	8.0	38.6	0.090	0.48	0.040	0	0.73	−0.10	5
AB	0.03	8.4	56.1	0.342	0.65	0.099	17.1	0.87	−0.07	2
TH	0.06	6.6	41.6	0.059	0.76	0.056	14.4	0.77	−0.19	6
LO	0.05	4.7	30.2	0.023	0.93	0.029	4.2	0.76	−0.13	11
BR	0.06	11.1	30.1	0	1.23	0.125	22.2	0.57	−0.21	46
BO	0.02	5.2	30.9	0	1.12	0	n/d	0.75	−0.24	9
CP	0	n/d	21.1	0.085	0.99	0	n/d	0.71	−0.10	5
Mean evergreen	*0.09*	*6.1*	*32.2*	*0.055*	*0.86*	*0.048*	*9.4*	*0.74*	*−0.15*	*18*
GU	0.44	8.9	24.8	0	0.41	0.043	0	0.84	−0.03	4
CL	2.55	8.4	31.0	0	0.55	0	n/d	0.79	−0.13	3
SO	0.16	8.5	33.3	0	1.07	0.033	0	0.59	−0.17	17
HE	0.31	11.2	32.4	0	0.93	0.020	0	0.69	−0.20	18
Mean deciduous	*0.38*[b]	*9.2*	*30.4*	*0*	*0.74*	*0.024*	*0*	*0.73*	*−0.13*	*10*
Mean all sites	*0.32*	*7.0*	*31.7*	*0.040*	*0.82*	*0.043*	*6.6*	*0.74*	*−0.15*	*16*

[a]Listed: the transition rate Δ/π (maximum relative rate of increase of assimilation rate A_s per °C temperature change), occurring at a crossover temperature T^*_{21} (mean over preceding 21 days), the theoretical maximum assimilation rate $A_{s,max}$, the vapor pressure deficit function parameter γ, the minimum base respiration rate $R_{0,min}$, and the proportionality constant a, which defines the increase in R_0 per unit A_s beyond a threshold assimilation capacity A^*_s. Further listed are model efficiency (E) for modeled and observed F_{NEE}, and the relative and absolute difference between mean fluxes. Here n/d denotes not defined. Values between brackets for Norunda are affected by an uncertain unit conversion error and were not included in calculating means.

[b]Median used instead of mean because of single high value for CL (see text).

number of times that the change in the fitted parameter value was positively or negatively related to a Q_{10} change, to indicate the possibility of uncertainty leading to bias.

[23] Parameter sensitivity describes how sensitive calculated F_{NEE} is to the value of each parameter. To investigate this, original parameter values for each site were independently decreased and increased by uncertainty U. The mean change in modeled F_{NEE} was calculated for all sites, and expressed as a fraction of original average F_{NEE}. Subsequently, dimensionless parameter sensitivity (S) was calculated as the relative change in mean F_{NEE} divided by the relative change in parameter value. This provides a first estimate of the model's sensitivity to different model parameters, although the actual value of S will have been influenced by the original parameter value, the magnitude and sign of the perturbation, and the original value of F_{NEE}.

[24] Finally, for each parameter the product of sensitivity and intersite variability can be seen as a measure of its importance in explaining NEE differences. We investigated this by multiplying the intersite coefficient of variation (CV, the ratio of standard deviation and mean) and sensitivity S of each parameter. The greater the resulting number, the more important a parameter is likely to be for explaining intersite NEE differences.

3. Results and Discussion

3.1. Explained Variance in Fluxes

[25] The fitted parameter values are listed in Table 2 together with indicators of model performance. Half-hourly model performance was generally good, with an overall mean model efficiency (E) of 0.74, varying between 0.57 (Brasschaat) and 0.87 (Aberfeldy). The overall difference between mean modeled and observed F_{NEE} rates was −0.15 μmol m^{-2} s^{-1}. This is a small value compared to typical instantaneous values, but corresponds to 0.57 t C ha^{-1} at an annual timescale. There was some negative bias in modeled F_{NEE} (16% on average, except for Norunda), which appeared to be related to short-lived but relatively large positive excursions in observed nighttime F_{NEE} that could not be accounted for by the model.

[26] Bi-weekly averages of observed and modeled NEE and its components are shown in Figure 1 for three selected sites, representing cases where half-hourly model performance was relatively good (Hyytiälä), average (Loobos), and poor (Sorø). Model performance for bi-weekly GPP, R, and NEE is not necessarily comparable to performance for half-hourly F_{NEE}. For Hyytiälä (Figure 1a), the model accurately described half-hourly variations in F_{NEE} (E = 0.83, Table 2) and bi-weekly GPP (E = 0.94) and R (E = 0.95), but bi-weekly NEE did not always agree that well (E = 0.69). The opposite is true for Sorø, where half-hourly F_{NEE} (E = 0.59) and bi-weekly R (E = 0.46) were reproduced relatively poorly, but bi-weekly GPP (E = 0.79) and NEE (E = 0.87) agreed well. GPP and R for this deciduous forest were underestimated or overestimated by equal amounts for much of the measurement period, particularly in late summer. For Loobos (Figure 1c) the model explained bi-weekly GPP (E = 0.92) and R (E = 0.79) better than either bi-weekly NEE (E = 0.70) or half-hourly F_{NEE} (E = 0.76).

[27] The temporal and intersite patterns in annual NEE, GPP, and R were explained reasonably well (model efficiencies were 0.70, 0.79, and 0.37, respectively), although modeled GPP and R were typically ∼15% lower than values estimated directly from F_{NEE} (Figure 2). The model

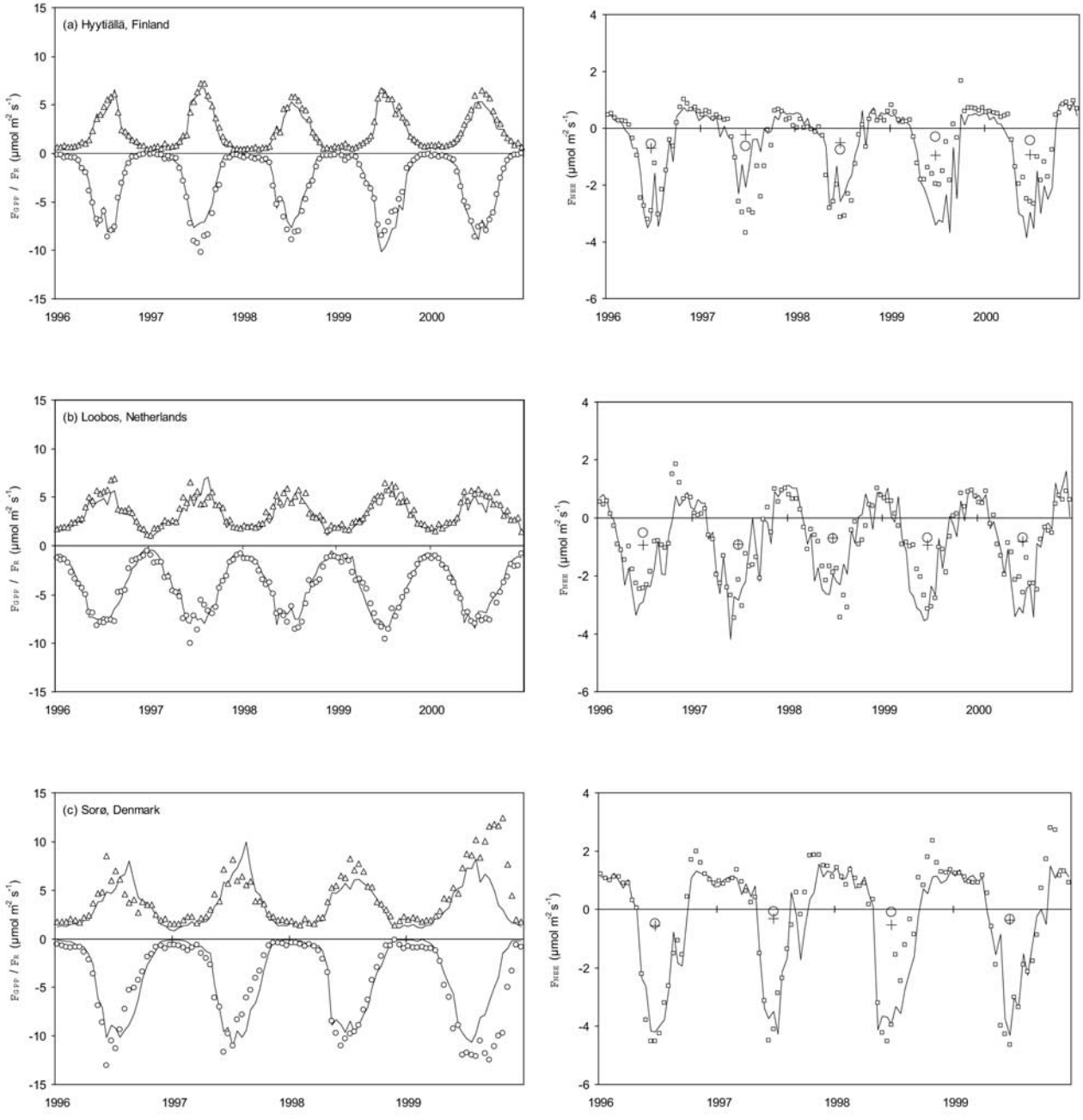

Figure 1. Temporal pattern in observed and modeled CO_2 fluxes at three EuroFlux sites. The symbols indicate (right) observed bi-weekly mean F_{NEE} (squares) and (left) its estimated components F_{GPP} (circles) and F_R (triangles), whereas the lines indicate values modeled with site-fitted parameters, for (a) an evergreen forest site with good model performance for half-hourly values (Hyytiälä, Finland; E = 0.83), (b) an evergreen forest site with average performance (Loobos, Netherlands; E = 0.76), and (c) a deciduous forest site showing relatively poor performance (Sorø, Denmark; E = 0.59). Also shown (right) are mean annual observed (circles) and modeled (pluses) values of F_{NEE}.

was initially developed using estimated F_{GPP} and F_R, but eventually fitted to the original F_{NEE} data, and therefore modeled and estimated GPP and R can vary substantially. In addition, the original F_{GPP} and F_R estimates are themselves subject to uncertainty, in particular related to low friction velocities (u^*) and the value of Q_{10} used in separating F_{GPP} and F_R (both typically 5–16% for total annual GPP and R [*Van Dijk and Dolman*, 2004]). In some cases, substantial gaps needed to be filled in both the observed and modeled time series, and this may have introduced further differ-

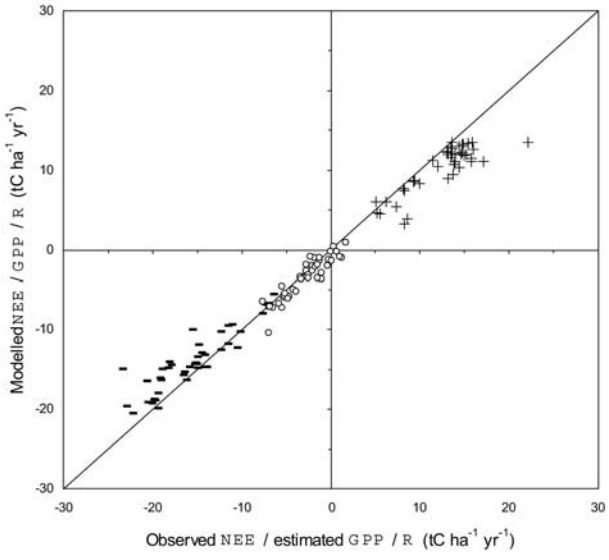

Figure 2. Plot of annual observed/estimated and modeled totals of NEE (circles), GPP (dashes) and R (crosses) (N = 43; Norunda and eight site-years for which >50% of data needed to be interpolated are omitted).

ences. Where climate data are available but F_{NEE} data are not, use of the model can be seen as an alternative, climate-sensitive method for the time-based gap-filling procedure used; it is not obvious which of the two is likely to provide better estimates [cf. *Falge et al.*, 2001].

3.2. Parameter Testing

[28] Deriving F_{GPP} and F_R estimates with different Q_{10} values and u^* thresholds did not affect the various steps in model development itself, and therefore the model structure itself appears robust (Appendix A). The chosen value of Q_{10} and u^* threshold both introduced a similar degree of uncertainty for each of the seven fitted model parameters (Table 3). Overall model efficiency E changed only slightly when using different Q_{10} values (by a mean 0.01) or u^* thresholds (mean 0.02) and showed increases as well as decreases.

[29] The (conservatively) estimated uncertainty in parameter values was greatest and most strongly biased for parameters describing base respiration and related to Q_{10} (39–121%, Table 3). This was expected, as scaling of respiration between reference temperature (0°C) and actual temperature depends directly on Q_{10} (see equation (1)), and therefore fitted base respiration values will be highly correlated to Q_{10}. Uncertainty U was modest for GPP parameters (4–15%), with the exception of the parameter describing the effect of vapor pressure deficit on assimilation rate (γ, 83–89%) (the implications of this are limited however; see section 3.4). Data selection and the Q_{10} value chosen might be expected to affect assimilation capacity values, since a higher estimate of daytime F_R should lead to higher F_{GPP} estimates, and ultimately greater assimilation capacity values should be fitted to these. In practice, this effect is small, because maximum assimilation rate was typically several times larger than the uncertainty in daytime respiration. Importantly, therefore, uncertainty in daytime F_R interpolation does not preclude the useful interpretation of F_{GPP} estimates [cf. *Van Dijk and Dolman*, 2004].

[30] The combined results of parameter uncertainty, sensitivity, and variability are listed in Table 4. The model was most sensitive to values for Q_{10} and maximum assimilation capacity ($A_{s,max}$). The three parameters related to R ($R_{0,min}$, a, and b) had the greatest effect on modeling results, not because they were particularly sensitive, but because their uncertainty was relatively large. For each parameter, the coefficient of intersite variation (CV) was multiplied with parameter sensitivity S to provide a first-order estimate of its relative importance in explaining differences in NEE between sites (Table 4). Again, maximum assimilation capacity ($A_{s,max}$, expressed per unit ground area) appeared to be the most important parameter, followed by the parameters describing the relationship between respiration rate and

Table 3. Calculated Uncertainty U (%) for the Model Parameters, Given Ranges of Q_{10} (1.6–2.5), and Friction Velocity (u^*) Threshold (0–0.5 m s^{-1})[a]

		Q_{10} Changed (1.6–2.5)		u^* Threshold Changed (0–0.5 m s^{-1})	
Parameter	Related to	Mean Uncertainty U, ±%	Positive/Negative Related	Mean Uncertainty U, ±%	Positive/Negative Related
f_α,[b] m^2 W^{-1}	GPP	4	2/0	10	1/1
Δ, °C^{-1}	GPP	14	6/18	13	10/13
T^*_{21}, °C	GPP	8	16/7	15	16/6
$A_{s,max}$, μmol m^{-2} s^{-1}	GPP	5	10/15	10	21/4
γ, kPa^{-1}	GPP	89	5/19	83	16/6
Q_{10}	R	–	–	11	17/11
$R_{0,min}$, μmol m^{-2} s^{-1}	R	39	5/11	16	9/6
a	R	66	0/18	24	13/5
b, μmol m^{-2} s^{-1}	R	121	12/6	73	4/14
Model efficiency (E)		0.01	2/27	0.02	23/5

[a]Listed: the resulting mean change from the original fitted parameter value (means for all sites) and the number of times that a change in Q_{10} or u^* led to a change in site fitted parameter value of equal or opposite sign (positive and negative related, respectively; total numbers are not necessarily equal, as some parameters may not have a value for all sites or were not changed at all by reanalysis). Also listed is the change in the fraction of variance explained (i.e., change in model efficiency E; see equation (7)).
[b]Fitted to all sites combined (see text).

Table 4. Results of Parameter Sensitivity Testing[a]

Parameter	Related to	Uncertainty U, %	Change in E	Change in F_{NEE}, %	Sensitivity S	Intersite CV	Relative Importance $S \times$ CV %
f_α, m^2 W^{-1}	GPP	7	−0.01	8	1.2	18[b]	30
Δ, °C^{-1}	GPP	14	0.00	1	0.1	99	10
T_{21}^*, °C	GPP	11	−0.01	7	−0.6	41	24
$A_{s,max}$, μmol m^{-2} s^{-1}	GPP	8	−0.01	15	1.9	36	69
γ, kPa^{-1}	GPP	86	0.00	4	0.0	207	10
Q_{10}	R	11[c]	−0.03	19	−1.7	25[d]	31
$R_{0,min}$, μmol m^{-2} s^{-1}	R	28	−0.01	13	−0.5	45	22
a	R	45	−0.04	42	−0.9	43	40
b, μmol m^{-2} s^{-1}	R	97	−0.03	29	−0.3	165	49

[a]Listed: estimated parameter uncertainty (U, taken as the average from the two values in Table 3), the change in mean model efficiency (E) and F_{NEE} for all sites after perturbing parameters by this uncertainty, and parameter sensitivity S (the ratio of the relative changes in F_{NEE} and the parameter value, respectively; positive values indicate an increase in modeled net uptake if parameter value is increased). Further listed are the intersite coefficient of variation (CV) for each parameter, and the product of CV and S, giving an estimate of the potential importance of each parameter in explaining intersite variations in NEE.

[b]Derived by regression analysis for individual sites.

[c]Uncertainty range assumed to equal Q_{10} range of 1.6–2.5 [cf. *Van Dijk and Dolman*, 2004].

[d]CV between calculated mean site Q_{10} values [from *Van Dijk and Dolman*, 2004] (conservative estimate).

assimilation capacity (notably a and b, Table 4). Forest characteristics that relate to different model parameters are discussed below.

3.3. Variation in Assimilation Capacity

[31] Forest phenology was described by a response curve between forest assimilation capacity and antecedent temperature (Figure 3; equation (4)). Intersite variation in parameters describing this curve could be attributed to forest functional type (evergreen or deciduous) and leaf area. Evergreen forest responded more slowly to seasonal changes in temperature than deciduous forests (Table 2, Figure 3). A noticeable exception was the fast transition in the northernmost evergreen forest (Flakaliden), which occurred at a crossover temperature that was considerably lower than for the other sites (T_{21}^* of 0.3°C versus 4°–11°C,

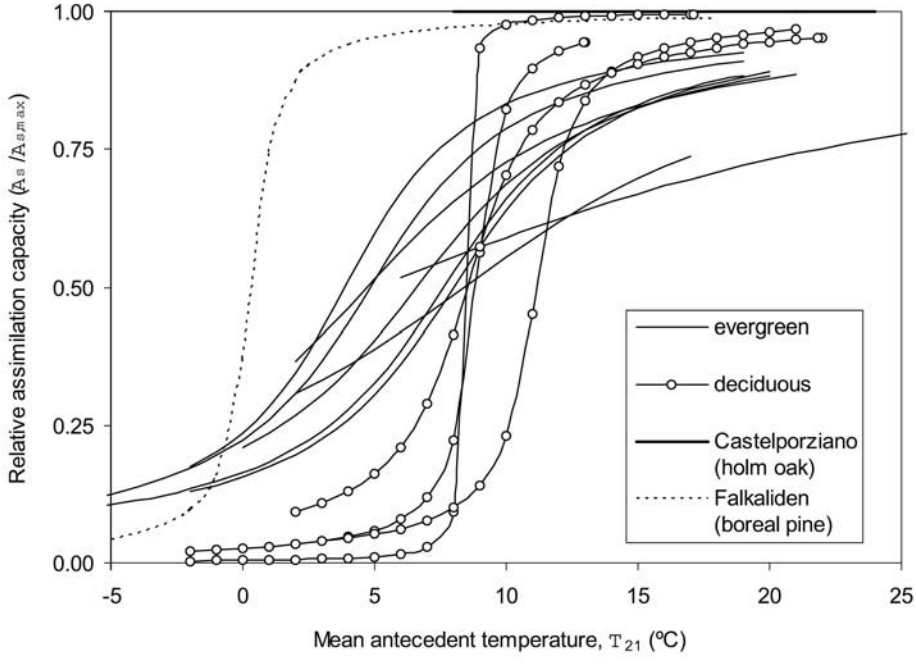

Figure 3. Relationship between mean temperature over the preceding 21 days (T_{21}) and relative assimilative capacity ($A_s/A_{s,max}$) as fitted to F_{NEE} data for the 15 EuroFlux forest sites for the observed range of T_{21}. Evergreen (solid line) and deciduous forests (line with circles) are shown separately, as are two atypical sites: Castelporziano (thick line: no apparent relationship) and Flakaliden (dashed line: fast transition at low temperature).

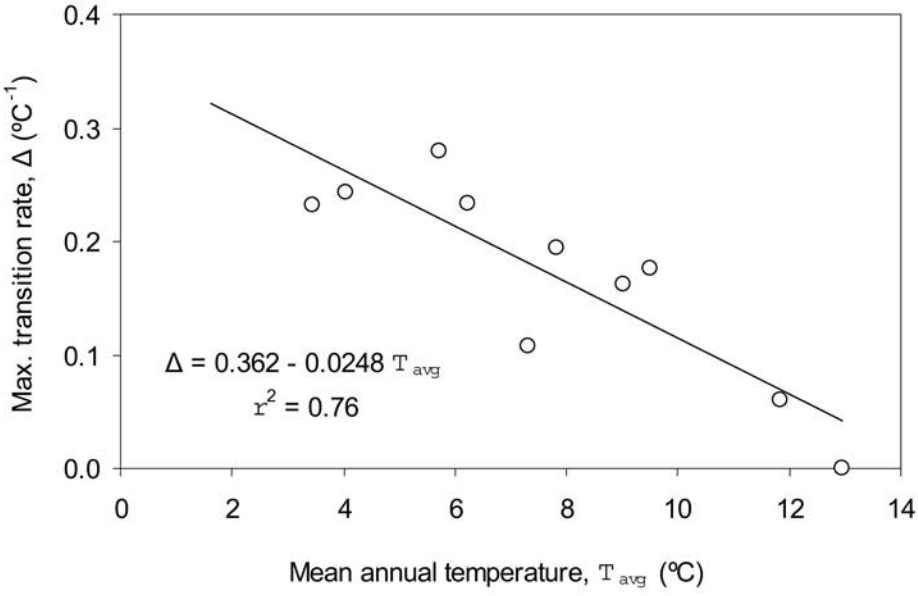

Figure 4. Relationship between average annual site temperature T_{avg} and the relative rate of assimilation capacity increase with temperature Δ for evergreen forests (excluding Flakaliden; see text).

Table 2) and seems to indicate a direct response to frost. There was a relationship between the relative transition rate Δ and average annual temperature T_{avg} for the remaining evergreen forests (Figure 4),

$$\Delta = 0.362 - 0.0248 T_{avg} \qquad r^2 = 0.76, N = 10. \qquad (8)$$

Equation (8) implies that forests in colder environments respond faster to temperature changes than forests in more a temperate climate, presumably to make optimum use of the growing season [cf. *Goulden et al.*, 1996; *Baldocchi et al.*, 2001]. Such a trend was not found for deciduous forests. We did not find an explanation for differences in crossover temperature, although T_{21}^* values for evergreen forests generally seemed somewhat lower (0°–11°C, mean 6.1°C) than for deciduous forest (9°–11°C, mean 9.2°C).

[32] The modeled phenological response to temperature agrees with earlier findings. For example, bud break in beech forests has been observed to occur once soil temperatures exceed 7°C [*Ellenberg*, 1988], which approximately agrees with the air temperature response observed in this study (Figure 3). Phenology may be driven by a wide variety of environmental cues (e.g., day length, soil temperature) and physiological processes (leaf aging, different responses in spring and fall). Previous studies suggest that antecedent temperature is a better indicator for leaf emergence, whereas senescence is often driven by day length and early frost [*Bondeau et al.*, 1999; *Barr et al.*, 2004]. The present description of phenology should be seen as a first approximation to capture only the most important of these factors without compromising model robustness and parameter efficiency.

[33] Fitted $A_{s,max}$ values are theoretical maximum values only. Actually modeled maximum values were up to ~30% lower (compare upper ends of curves in Figure 3) and agree reasonably well with reported values, although these are derived differently [e.g., *Pilegaard et al.*, 2001; *Falge et al.*, 2002; *Carrara et al.*, 2004]. The maximum modeled $A_s(i)$

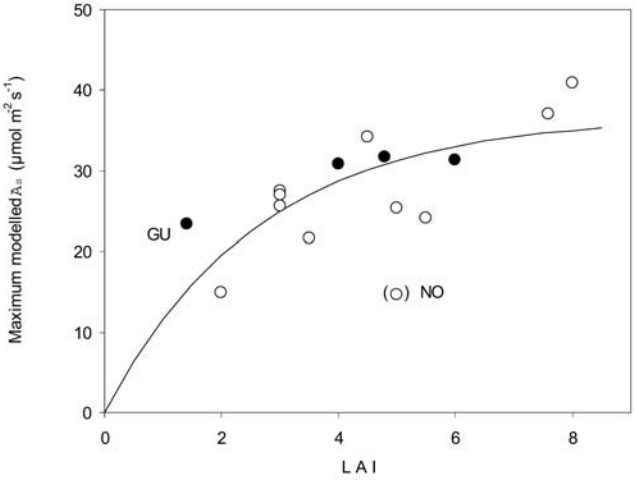

Figure 5. Relationship between leaf area index (LAI) and the maximum modeled value of assimilation capacity (i.e., A_s for the highest observed T_{21}), together with a fitted exponential saturation function (equation (9), r^2 = 0.53). Evergreen forests are indicated by open circles; deciduous forests are indicated by closed circles. GU, Gunnarsholt; NO, Norunda (shown between brackets because of an uncertain unit conversion error)).

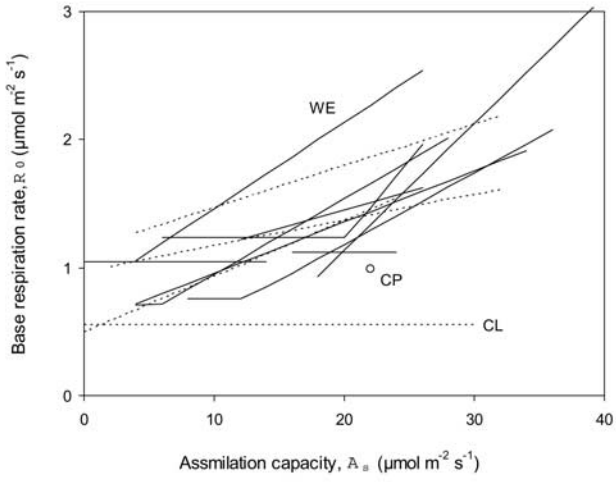

Figure 6. Fitted relationships between base respiration rate R_0 and maximum assimilation capacity A_s for the 15 sites. Shown are evergreen forests (solid lines), deciduous forests (dotted lines), and the single optimized R_0 value for Castelporziano (CP, open circles). CL, Collelongo; WE, Weidenbrunnen.

value could be related to leaf area index L^* by an exponential function (Figure 5),

$$\max[A_s(i)] = 36.8\left[1 - \exp\left(-0.38L^*\right)\right] \qquad r^2 = 0.53, N = 14. \tag{9}$$

The r^2 of equation (9) was improved to 0.65 after excluding the Gunnarsholt cottonwood plantation, which was much lower (1 m) and denser (10,000 ha^{-1}) than the other forests [*Valentini*, 2003]. Equation (9) looks similar to the Lambert-Beer function, but the coefficient is lower than light extinction coefficients of 0.6–0.7 typically found for forests. This implies that assimilation capacity does not increase linearly with light interception [cf. *Stitt and Schulze*, 1994].

[34] The correlation between LAI and assimilation capacity may have been positively or negatively affected by several factors. Artificial causes include the fact that reported LAI values (1) were determined by different techniques; (2) were usually reported to the next 0.5 or 1 unit; (3) may not have been representative for the average flux footprint; (4) typically represent a one-time measurement that probably differs from the maximum LAI value during the observation period [cf. *Barr et al.*, 2004]; and (5) do not include undergrowth (important for the sparse forests of Gunnarsholt, Flakaliden, and Castelporziano). Genuine causes for variation in the relationship between LAI and assimilation capacity may include forest species composition, age, management history, soil properties, and nutrient availability. These will affect relationships between leaf biomass, leaf area, and leaf assimilative capacity, while the spatial distribution of leaf biomass can also differ [*Norman and Jarvis*, 1974]. Some of the leaf area variation among forests can be explained by climate: The low Mediterranean forest LAI is presumably related to water limitations, and the low leaf area for the three northernmost forests (1.4–3, Table 1) is typical for these latitudes.

3.4. Response to Vapor Pressure Deficit and Water Availability

[35] The parameter γ, describing the effect of vapor pressure deficit on F_{GPP}, varied between 0 and 0.34 kPa^{-1} among the sites (mean 0.040 kPa^{-1}). For the six sites for which a γ value was fitted, an indication of the effect of air humidity on NEE was obtained by omitting the humidity response function. The resulting increase in modeled net uptake was substantial for Aberfeldy, Castelporziano, Tharandt, and Vielsalm (8–12%; 0.4–0.6 t C ha^{-1} yr^{-1}), but small for Hyytiälä and Loobos (2–4%, <0.1 t C ha^{-1} yr^{-1}). This corroborates previous findings that the overall effect of air humidity on temperate and boreal European forest NEE is limited [*Schulze and Hall*, 1982] (but see *Dolman et al.* [2004]). Estimated soil water contents also did not assist much in explaining temporal variations in F_{NEE} during model development (Appendix A), but (1) the period of data collection (1996–2000) did not include extreme events like the dry summer of 2003 [*Schär et al.*, 2004]; (2) our data set included only one Mediterranean forest (Castelporziano); and (3) water limitation may be expressed in adapted ecosystem structure and functioning that anticipates rather than responds to dry conditions [cf. *Fotelli et al.*, 2000; *López et al.*, 2001]. The low LAI (3.5) of the Mediterranean forest at Castelporziano may reflect limited water availability, and *Reichstein et al.* [2002] did find a significant effect of hydrology on ecosystem carbon fluxes in this and two other Mediterranean forests.

3.5. Variation in Respiration

[36] Our estimates of GPP and R, and the model based on these, show high assimilation capacity and rates coinciding with high (base) respiration rates [cf. *Van Dijk and Dolman*, 2004; *Carrara et al.*, 2004]. Base respiration (R_0) (including autotrophic and heterotrophic contributions) could be expressed as the sum of a constant component ($R_{0,min}$) and a component that increased in proportion to assimilative capacity A_s (equation (5), Figure 6). The forest at Weidenbrunnen showed considerably higher base respiration rates than the other sites, possibly related to the observed forest decline [*Rebmann et al.*, 2004]. For a number of forests, fitting the two-domain model led to a simpler relationship, either because (1) high (Flakaliden) or low (Aberfeldy) assimilation rates did not occur; (2) variation in fitted assimilation rate was small (Bordeaux) or none (Castelporziano); (3) the data suggested a monotonic increase of R_0 with A_s (three of the four deciduous forests, although visual data inspection still suggested two domains; Figure 6); or (4) R_0 did not seem related to assimilative capacity at all (the fourth deciduous forest at Collelongo).

[37] The method of data selection and F_{GPP} and F_R separation did not affect the general form of the relationship between R_0 and A_s, although it did change the actual parameter values (section 3.2). Equation (5) expresses a purely statistical relationship that integrates the sum of

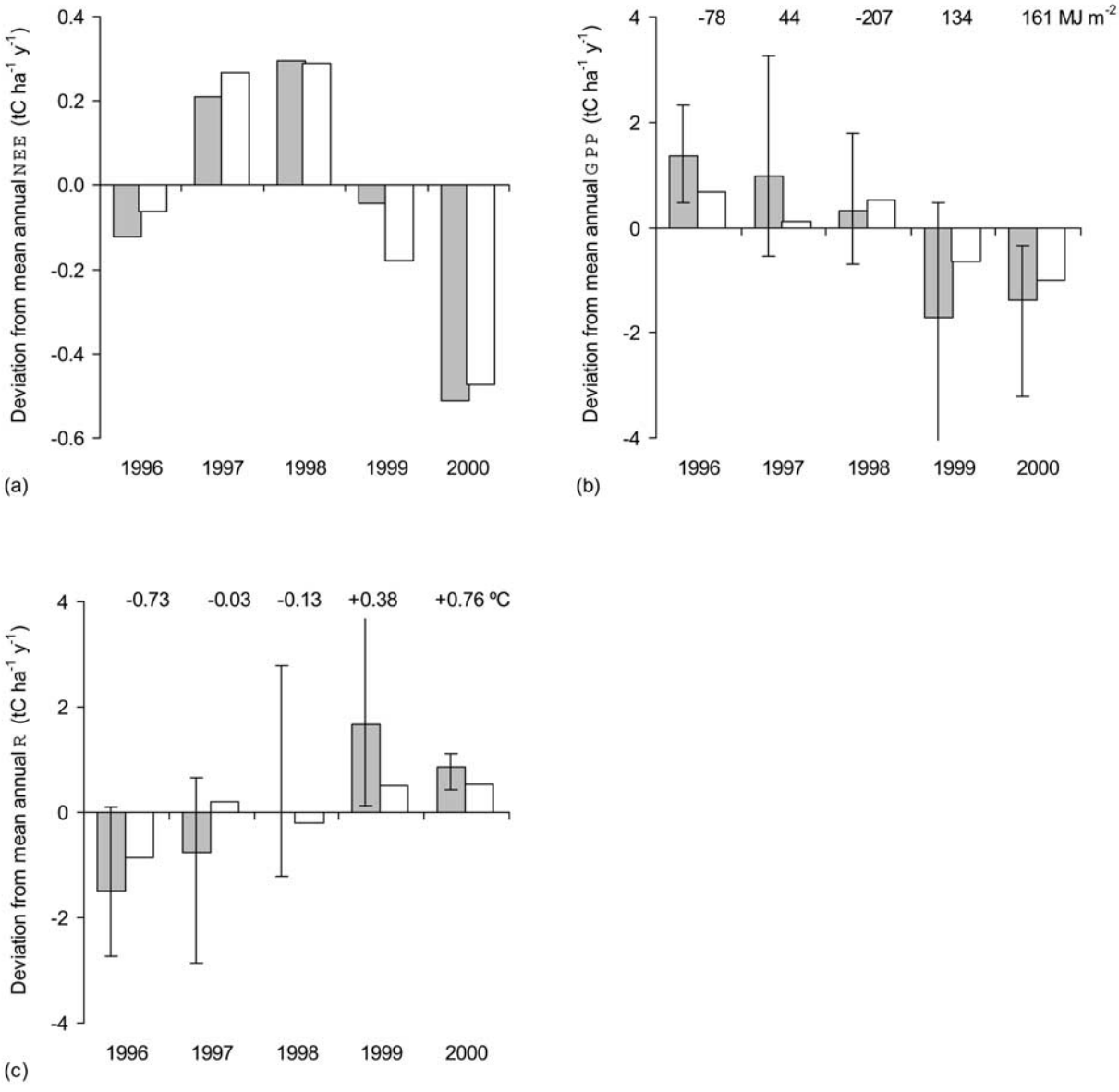

Figure 7. Annual deviations from mean (a) NEE, (b) GPP, and (c) R for the six sites with 4–5 years of data. Shaded bars show mean deviation of observed values (range indicated by vertical lines, except for NEE because of scale difference); white bar shows modeled deviation. Average radiation and temperature deviations are listed for comparison in Figures 7b and 7c, respectively.

comparably sized respiration fluxes from the foliage, wood, roots and heterotrophic (soil) organisms (section 2.2). A direct relationship between tree maintenance respiration rate and assimilation capacity may well exist, in particular for the foliage. Soil respiration has been shown to be strongly related to actual assimilation [*Högberg et al.*, 2001]. Heterotrophic respiration may be directly linked to GPP through root exudates, mycorrhizae, and biomass turnover, and indirectly correlated to it because soil biological activity follows a similar seasonal pattern. To this should be added the complex interaction between soil temperature at different depths (affecting soil respiration rate and tree phenology, and through this also aboveground base respiration) and air temperature (affecting aboveground respiration) [*Bernhofer et al.*, 2003]. Part of the unexplained variation in respiration may be attributable to differences in the relative importance of these component fluxes between seasons [*Falge et al.*, 2003; *Rebmann et al.*,

2004] and sites (e.g., related to soil and litter layer characteristics, soil hydrology, and historical and current soil management).

3.6. Main Factors Explaining Interannual Variations in NEE, GPP, and R

[38] The interannual variation in total NEE for individual sites was not well explained by the model (see Figure 1). Annual net NEE is the small net balance between net uptake in summer and net release in winter, and therefore small differences between modeled and observed NEE at subannual timescales can become important at the annual scale. Apart from model inadequacies, potential causes for unexplained NEE variation include infrequent events (insect pests, disease outbreaks, severe weather), occasional or persistent human disturbance within the footprint, and measurement bias or errors (e.g., small changes in the instruments or setup).

[39] If the lack of agreement between observed and modeled interannual NEE is due to unaccounted local events or transient conditions, one would expect that the average interannual pattern for multiple sites is still reproduced. We compared the interannual variation in observed and modeled NEE and its components, for six sites that had 4–5 years of data (Hyytiälä, Sorø, Loobos, Tharandt, Hesse, and Weidenbrunnen; Table 1). Averaging fluxes for these six sites will not represent any particular spatial scale, but emphasizes common variations in uptake and release that may be related to large-scale climate variations, while suppressing local causes. Most of the interannual patterns in NEE, GPP, and R were indeed reproduced (Figure 7). The warmer but brighter years 1999 and 2000 showed greater GPP and R than the cooler but dimmer years 1996–1998 (Figures 7a–7c). The same pattern was found for net uptake, with the exception of 1996. Overall, interannual variations of radiation therefore seemed to dominate over temperature in the net carbon balance [*Schulze*, 1970]. To further test this contention, we independently and uniformly changed all instantaneous radiation and temperature measurements by the variation in annual average values (±6% for radiation, and −0.7°C to +0.8°C for temperature). Increasing radiation inputs caused an average NEE change of 7% by increasing GPP in the model. Increasing temperature caused an increase in overall assimilation capacity and therefore GPP (see Figure 3), but also increased R because of the greater assimilation rates (see Figure 6), and because of the direct temperature response (equation (1)). Higher temperatures increased R more than GPP, and the cited temperature deviations changed average annual NEE by 3%. This supports our earlier conclusions and also suggests that without acclimation or a change in radiation, uniformly higher temperatures during warmer years alone may not increase carbon uptake.

3.7. Main Factors Explaining Intersite Variations in NEE, GPP, and R

[40] The previous sections together suggest that radiation, temperature, and leaf area explain most of the variation in GPP, R, and NEE between sites. To further test this, we performed a stepwise regression between normal and log-transformed mean annual values of the respective fluxes, global radiation (Q_{avg} in GJ yr^{-1}), and temperature (T_{avg}), and reported LAI values (L^*) for 13 out of 15 sites (Table 1; Norunda was excluded, as well as Gunnarsholt, for which the radiation time series could not be gap-filled). Simple regression equations indeed explained considerable variation in GPP and R, and to a lesser extent in their smaller net balance NEE (the total variance explained after each step is also listed),

$$GPP = -5.13\ln(L^*) - 2.13\ln(Q_{avg}) - 3.29\ln(T_{avg}) + 0.33$$
$$r^2 = \quad 0.66 \rightarrow \quad 0.75 \rightarrow \quad 0.86, \qquad (10a)$$

$$R = 4.87\ln(T_{avg}) - 1.98\ln(Q_{avg}) - 2.35\ln(L^*) + 7.37$$
$$r^2 = \quad 0.67 \rightarrow \quad 0.75 \rightarrow \quad 0.83, \qquad (10b)$$

$$NEE = -10.5\ln(Q_{avg}) - 0.610\ln(L^*) + 1.63\ln(T_{avg}) + 9.85$$
$$r^2 = \quad 0.28 \rightarrow \quad 0.39 \rightarrow \quad 0.45. \qquad (10c)$$

We do not propose that these simple regressions provide evidence by themselves, but they reinforce our finding that radiation, temperature, and leaf area are the drivers of NEE in central and northern European forests, and that GPP dominates R in this balance [*Van Dijk and Dolman*, 2004; *Janssens et al.*, 2001].

4. Conclusions

[41] We used half-hourly NEE data collected at 15 European sites in a stepwise regression approach to develop an empirical NEE model that incorporates existing physiological concepts and process formulations. We subsequently used the model to analyze temporal and intersite NEE variations. The developed model was robust despite uncertainties in Q_{10} and friction velocity threshold (section 3.2), and accurately explained temporal NEE patterns at timescales of half hours to seasons (section 3.1). Radiation and temperature were the dominant climate variables in explaining NEE variations. Vapor pressure deficit and soil moisture did not appear to have a large effect on NEE, but the data set analyzed was biased toward wetter sites and years (section 3.4). Maximum assimilation capacity was the forest characteristic most powerful in explaining NEE variations across sites, and in turn, could be related to forest leaf area (section 3.3). Both temporal and intersite variations in respiration were closely related to GPP. This purely statistical relationship may have a complex background including direct, indirect, and spurious components (sections 3.5 and 3.7).

[42] The model did not explain interannual patterns in GPP, R, and NEE for individual sites, but did reproduce the average pattern for six sites. The temporal variability in GPP is greater than that in R, and GPP dominated interannual NEE patterns. Radiation and temperature appear to be the main drivers of (large-scale) interannual NEE variation for the studied forests and period. Radiation dominated

temperature, to the effect that brighter but warmer years tended to show higher net uptake than cooler but dimmer ones (section 3.6). Annual mean temperature, radiation, and forest leaf area already explained 45% of the intersite variation in NEE, 86% of the variation in GPP, and 83% of the variation in R (section 3.7). Summarizing, our results suggest that global radiation and temperature, modified by leaf area, explain most of the NEE variation among northern and central European forests, and are the main drivers of the observed latitudinal gradient and (large-scale) interannual patterns in GPP, R, and NEE.

Appendix A: Model Development

[43] The NEE model used in this paper was derived by stepwise regression analysis of F_{GPP} and F_R estimates based on the EuroFlux data set [*Falge et al.*, 2001; *Van Dijk and Dolman*, 2004]. The order and type of model selection (and therefore also the number of parameters) was informed by existing physiological knowledge where this was available. Otherwise, the concept used was similar to Akaike's Information Criterion (AIC): A new model component was accepted if it explained at least 2% of additional variance in half-hourly GPP or R. For example, it was obvious a priori that the diurnal course in NEE needed to be explained first, that this was primarily driven by radiation, and that a hyperbolic model (requiring two or more parameters) could accurately describe the relationship. We used the 2% criterion to decide on alternative model formulations, and to reduce the number of fitting parameters where parameters were correlated (as for the example given). The full procedure was repeated after separating F_{GPP} and F_R with Q_{10} values of 1.6 and 2.5, respectively, instead of the original 2.0. This changed the coefficient of determination and parameters of the regression equations in many cases (see main text), but not the basic structure of the model. The model was developed as outlined below.

[44] The relationship between global radiation Q and estimated F_{GPP} was analyzed by fitting a Michaelis-Menten type equation [cf. *Hollinger et al.*, 1994] for half-hourly data (i) pooled per month (m),

$$F_{GPP}(i,m) = \frac{\alpha(m) A_s(m) Q(i,m)}{A_s(m) + \alpha(m) Q(i,m)} + \varepsilon_{GPP}(m), \qquad \text{(A1)}$$

where α(μmol J^{-1}) is ecosystem light use efficiency, A_s (μmol m^{-2} s^{-1}) is the assimilation rate under light-saturated conditions, and Q (W m^{-2}) is global radiation. The term ε_{GPP} (μmol m^{-2} s^{-1}) is a residual term comprising additional variation that may be explained by variables to be introduced in the next regression steps, remain unexplained due to model inadequacy, be caused by errors in estimating F_{GPP} from observed F_{NEE}, or be caused by measurement bias. In most cases, equation (A1) fitted F_{GPP} estimates well. For 89% of all site-months ($N = 498$) >50% of variance was explained, with 42% showing $r^2 > 0.6$ and a single highest value of $r^2 = 0.91$. Similar numbers of positive and negative mean values were found for ε.

[45] For many sites, visual inspection suggested a proportional relationship between monthly values of light use efficiency α and light-saturated assimilation rate A_s [*Pilegaard et al.*, 2001; *Carrara et al.*, 2004], although strong relationships ($r^2 > 0.7$) were only found for three out of 15 sites. The relationship between α and A_s for all monthly values (means for multiple years were used for equal weighting) was described by a constant of proportionality $f_\alpha = \alpha/A_s$ (m^2 W^{-1}) of 0.0042 ($r^2 = 0.56$, $N = 130$). This finding was used to simplify equation (A1) to

$$F_{GPP}(i) = \frac{f_\alpha A_s(m) Q(i)}{1 + f_\alpha Q(i)} + \varepsilon(i). \qquad \text{(A2)}$$

[46] Use of equation (A2) simplifies model parameterization considerably and solves problems of overparameterization caused by the correlation between α and A_s. It performed very similarly to equation (A1): Site mean r^2 values were decreased by 0.008 only, while a decrease of 0.02 occurred for only two sites. The direct relationship between α and A_s is consistent with biophysical theory if the variation in α and A_s between months at ecosystem level are both driven primarily by canopy development. The value of $1/f_\alpha \approx 240$ W m^{-2} may be interpreted as the radiation saturation point and is close to literature values for individual, well-lit leaves [e.g., *Eagleson*, 2002].

[47] The residual difference (ε_{GPP}) between estimated F_{GPP} and values modeled with equation (A2) was normalized through division by fitted monthly A_s. Both absolute and normalized residuals were compared to (1) instantaneous air temperature T (°C), (2) the ratio of Q over calculated extraterrestrial radiation S_0 (W m^{-2}) as a measure of the amount of direct versus diffuse radiation [*Law et al.*, 2002], and (3) vapor pressure deficit D (kPa). For eight out of 15 sites, D explained a significant part of ε_{GPP}. We did not find significant correlation between the remaining variation and either temperature or diffusivity, possibly because previously found relationships primarily express the correlation of these variables with D [cf. *Carrara et al.*, 2004]. The decrease of F_{GPP} per kPa change in D appeared greatest at low D, and was described by equation (3) [cf. *Schulze and Hall*, 1982; *Leuning*, 1995] with one parameter (γ).

[48] We fitted equation (3) to F_{GPP} estimates pooled per day but using a single, optimized γ value for each site. This removed the effects of D and Q and produced best fit daily A_s values. We investigated the correlation between these daily A_s values and the mean temperature (T_N) over the preceding N (1–60) days. In most cases, moderate to good correlation ($r^2 = 0.45$–0.80) existed with the mean temperature over the preceding 2–5 weeks. For evergreen forests, the optimum averaging period length roughly decreased with increasing mean annual temperature, with optima of about 1 month for the three boreal sites to less than a week for the two warmest sites (Bordeaux and Castelporziano). The degree of correlation also roughly decreased in this order. For deciduous forests, the best period of averaging was in the order of 1 month in all four cases. To assess how well the optimum period lengths were defined for the

15 sites, we determined the range of N days for which correlation between A_s and T_N deteriorated by <0.02. This helped us decide upon the best common denominator and suggested the mean temperature over the preceding 21 days (T_{21}) as a useful compromise. The tangential curve described by equation (4) fitted the daily T_{21}-A_s pairs well for all forests except the evergreen holm oak forest at Castelporziano. We compared the difference between weekly modeled and estimated mean F_{GPP} and F_R with an index of soil moisture availability to investigate if either was suppressed (see *Van Dijk and Dolman* [2004] for details). We did not find a consistent relationship between soil moisture index values and the difference between mean weekly modeled and estimated F_{GPP} for any site, and therefore did not include this effect in our model.

[49] We compared both daily and monthly values of calculated base respiration (R_0) with values of GPP, T_{21}, and mean values of fitted A_s on these timescales. For most sites, both the monthly and daily fitted values of R_0 were correlated to A_s and showed two domains: a constant R_0 value below a threshold A_s, and R_0 values that increased proportionally to A_s above this threshold. Not all sites showed a two-domain relationship, but all cases could be described by equation (5).

[50] **Acknowledgments.** The authors gratefully acknowledge the collection and provision of data by the EC's CarboEurope Integrated Project, and in particular site researchers A. Aubinet, P. Berbigier, C. Bernhofer, R. Ceulemans, A. Granier, P. Jarvis, N. O. Jensen, A. Lindroth, D. Loustau, G. Matteucci, J. Moncrieff, E. J. Moors, K. Pilegaard, C. Rebmann, H. Thorgeirsson, R. Valentini, and T. Vesala, and E. Falge, who processed the EuroFlux data set and provided important background information. This work was funded by a grant from the Netherlands Organization for Scientific Research (NWO), which is gratefully acknowledged. We also thank the various reviewers of earlier versions of this manuscript.

References

Aubinet, M., et al. (2000), Estimates of the annual net carbon and water exchange of forests: The EuroFlux methodology, *Adv. Ecol. Res.*, *30*, 113–176.

Baldocchi, D., et al. (2001), FLUXNET: A new tool to study the temporal and spatial variability of ecosystem-scale carbon dioxide, water vapor, and energy flux densities, *Bull. Am. Meteorol. Soc.*, *82*, 2415–2433.

Barr, A. G., T. A. Black, E. H. Hogg, N. Kljun, K. Morgenstern, and Z. Nesic (2004), Inter-annual variability in the leaf area index of a boreal aspen-hazelnut forest in relation to net ecosystem production, *Agric. For. Meteorol.*, *126*, 237–255.

Bernhofer, C., M. Aubinet, R. Clement, A. Grelle, T. Grünwald, A. Ibrom, P. Jarvis, C. Rebmann, E.-D. Schulze, and J. D. Tenhunen (2003), Spruce forests (Norway and Sitka spruce, including Douglas fir): Carbon and water fluxes, balances, ecological and ecophysiological determinants, in *Fluxes of Carbon, Water and Energy of European*, *Ecol. Stud. Ser.*, vol. 163, edited by R. Valentini, pp. 99–124, Springer, New York.

Bondeau, A., D. W. Kicklighter, J. Kaduk, and the participants of the Potsdam NPP model Intercomparison (1999), Comparing global models of terrestrial net primary productivity (NPP): Importance of vegetation structure on seasonal NPP estimates, *Global Change Biol.*, *5*, 35–45.

Carrara, A., I. A. Janssens, J. C. Yuste, and R. Ceulemans (2004), Seasonal changes in photosynthesis, respiration and NEE of a mixed temperate forest, *Agric. For. Meteorol.*, *126*, 15–31.

Dolman, A. J., T. C. Maximov, E. J. Moors, A. P. Maximov, J. A. Elbers, A. V. Kononov, M. J. Waterloo, and M. K. van der Molen (2004), Net ecosystem exchange of carbon dioxide and water of far eastern Siberian Larch (Larix dahurica) on permafrost, *Biogeosci. Disc.*, *1*, 275–309.

Eagleson, P. S. (2002), *Ecohydrology: Darwinian Expression of Form and Function*, 443 pp., Cambridge Univ. Press, New York.

Ellenberg, H. (1988), *Vegetation Ecology of Central Europe*, 4th ed., Cambridge Univ. Press, New York.

Falge, E., et al. (2001), Gap filling strategies for defensible annual sums of net ecosystem exchange, *Agric. For. Meteorol.*, *107*, 43–69.

Falge, E., et al. (2002), Seasonality of ecosystem respiration and gross primary production as derived from FLUXNET measurements, *Agric. For. Meteorol.*, *113*, 53–74.

Falge, E., et al. (2003), A model-based study of carbon fluxes at ten European forest sites, in *Fluxes of Carbon, Water and Energy of European Forests*, *Ecol. Stud. Ser.*, vol. 163, edited by R. Valentini, pp. 151–177, Springer, New York.

Fotelli, M. N., K. M. Radoglou, and H.-I. A. Constantinidou (2000), Water stress responses of seedlings of four Mediterranean oak species, *Tree Physiol.*, *20*, 1065–1075.

Goulden, M. L., J. W. Munger, S.-M. Fan, B. C. Daube, and S. C. Wofsy (1996), Exchange of carbon dioxide by a deciduous forest: Response to inter-annual climate variability, *Science*, *271*, 1576–1578.

Högberg, P., A. Nordgren, N. Buchmann, A. F. S. Taylor, A. Ekblad, M. N. Högberg, G. Nyberg, M. Ottosson Löfvenius, and D. J. Read (2001), Large-scale forest girdling shows that current photosynthesis drives soil respiration, *Nature*, *411*, 789–792.

Hollinger, D. Y., F. M. Kelliher, J. N. Byers, J. E. Hunt, T. M. McSeveny, and P. L. Weir (1994), Carbon dioxide exchange between an undisturbed old-growth temperate forest and the atmosphere, *Ecology*, *75*, 143–150.

Intergovernmental Panel on Climate Change (2001), *Climate Change 2001: The Scientific Basis*, 881 pp., Cambridge Univ. Press, New York.

Janssens, I. A., and K. Pilegaard (2003), Large seasonal changes in Q_{10} of soil respiration in a beech forest, *Global Change Biol.*, *9*, 911–918.

Janssens, I. A., et al. (2001), Productivity and disturbance overshadow temperature in determining soil and ecosystem respiration across European forests, *Global Change Biol.*, *7*, 269–278.

Janssens, I. A., et al. (2003), Europe's terrestrial biosphere absorbs 7 to 12% of European anthropogenic CO_2 emissions, *Science*, *300*, 1538–1542.

Knorr, W., and M. Heimann (2001), Uncertainties in global terrestrial biosphere modeling: 1. A comprehensive sensitivity analysis with a new photosynthesis and energy balance scheme, *Global Biogeochem. Cycles*, *15*, 207–225.

Law, B. E., et al. (2002), Environmental controls over carbon dioxide and water vapor exchange of terrestrial vegetation, *Agric. For. Meteorol.*, *113*, 97–120.

Lechowicz, M. J. (1984), Why do temperate deciduous trees leaf out at different times? Adaptation and ecology of forest communities, *Am. Nat.*, *124*, 821–842.

Leuning, R. (1995), A critical appraisal of a combined stomatal-photosynthesis model for C3 plants, *Plant Cell Environ.*, *18*, 339–355.

Lloyd, J., and J. A. Taylor (1994), On the temperature dependence of soil respiration, *Funct. Ecol.*, *8*, 315–323.

López, B., S. Sabaté, and C. A. Gracia (2001), Fine-root longevity of *Quercus ilex*, *New Phytol.*, *151*, 437.

Nabuurs, G. J., A. Pussinen, T. Karjalainen, M. Erhard, and K. Kramer (2002), Increment changes in European forests due to climate change, *Global Change Biol.*, *8*, 1–13.

Norman, J. M., and P. G. Jarvis (1974), Photosynthesis in Sitka spruce: III. Measurements of canopy structure and radiation environment, *J. Appl. Ecol.*, *11*, 375–398.

Pilegaard, K., P. Hummelshoj, N. O. Jensen, and Z. Chen (2001), Two years of continuous CO_2 eddy-flux measurements over a Danish beech forest, *Agric. For. Meteorol.*, *107*, 29–41.

Rebmann, C., et al. (2004), Carbon budget of a spruce forest ecosystem, in *Biogeochemistry of Forest Catchments in a Changing Environment*, *Ecol. Stud. Ser.*, vol. 172, edited by E. Matzner, pp. 143–159, Springer, New York.

Reichstein, M., J. D. Tenhunen, O. Roupsard, J.-M. Ourcival, S. Rambal, F. Miglietta, A. Peressotti, M. Pecchiari, G. Tirone, and R. Valentini (2002), Severe drought effects on ecosystem CO_2 and H_2O fluxes in three Mediterranean evergreen ecosystems: Revision of current hypotheses?, *Global Change Biol.*, *8*, 999–1017.

Schär, C., P. L. Vidale, D. Luthi, C. Frei, C. Haberli, M. A. Liniger, and C. Appenzeller (2004), The role of increasing temperature variability in European summer heat waves, *Nature*, *427*, 332–336.

Schulze, E.-D. (1970), Der CO_2-Gaswechsel der Buche (*Fagus silvatica* L.) in Abhängigkeit von den Klimafaktoren im Freiland, *Flora*, *159*, 177–232.

Schulze, E.-D. (1986), Carbon dioxide and water vapor exchange in response to drought in the atmosphere and in the soil, *Annu. Rev. Plant Physiol.*, *37*, 247–274.

Schulze, E.-D., and A. E. Hall (1982), Stomatal responses, water loss and CO_2 assimilation rates of plants in contrasting environments, in *Encyclo-*

pedia of Plant Physiology, *New Ser.*, vol. 12B, edited by O. L. Lange et al., pp. 181–230, Springer, New York.

Sitch, S., et al. (2003), Evaluation of ecosystem dynamics, plant geography and terrestrial carbon cycling in the LPJ dynamic global vegetation model, *Global Change Biol.*, *9*, 161–185.

Stitt, M., and E.-D. Schulze (1994), Plant growth, storage, and resource allocation: From flux control in a metabolic chain to the whole plant level, in *Flux Control in Biological Systems: From Enzymes to Populations and Ecosystems*, edited by E.-D. Schulze, pp. 57–118, Elsevier, New York.

Valentini, R. (Ed.) (2003), *Fluxes of Carbon, Water and Energy of European Forests*, *Ecol. Stud. Ser.*, vol. 163, Springer, New York.

Valentini, R., et al. (2000), Respiration as the main determinant of carbon balance in European forests, *Nature*, *404*, 861–865.

Van Dijk, A. I. J. M., and A. J. Dolman (2004), Estimates of CO_2 uptake and release among European forests based on eddy covariance data, *Global Change Biol.*, *10*, 1445–1459.

H. Dolman, Department of Hydrology and Geo-Environmental Sciences, Faculty of Earth and Life Sciences, Vrije Universiteit Amsterdam, De Boelelaan 1085, NL-1081 HV, Amsterdam, Netherlands.

E.-D. Schulze, Max Planck Institute for Biogeochemistry, P.O. Box 100164, D-07701 Jena, Germany.

A. I. J. M. van Dijk, CSIRO Land and Water, GPO Box 1666, Canberra, ACT 2601, Australia. (albert.vandijk@csiro.au)